International Communications in Heat and Mass Transfer 39 (2012) 509–513

Contents lists available at SciVerse ScienceDirect

International Communications in Heat and Mass Transfer

journal homepage: www.elsevier.com/locate/ichmt

# An investigation of natural convection in a three dimensional tapered chimney without Boussinesq assumption ☆

Wu-Shung Fu *, Yun Huang, Wei-Hsiang Wang

*Department of Mechanical Engineering, National Chiao Tung University, Hsinchu 30010, Taiwan, ROC*

ARTICLE INFO

Available online 30 January 2012

*Keywords:*
Tapered chimney
Compressible natural convection
Without Boussinesq assumption

ABSTRACT

Natural convection in a three dimensional tapered chimney is investigated numerically. In order to investigate the natural convection under a high temperature difference situation, Boussinesq assumption is not adopted instead of consideration of the compressibility of fluid. Methods of Roe scheme, preconditioning and dual time stepping are used to solve governing equations for a low speed compressible flow. Coordinates transformation of algebraic grid generation and non-reflecting boundary condition are used to facilitate computation processes. The results reveal that in the expanding duct local Nusselt numbers distributed around the corner region are larger than those distributed around the central region. An available correlation equation is proposed and is well consistent with the numerical results.



## 1. Introduction

It is well-known, a structure of chimney is indispensably used in high temperature systems of combustion, pollution control, ventilation, etc. That the importance of practical application of the chimney is indisputable is the main reason for the study of heat transfer mechanisms of the chimney still receiving lots of attentions.

Basically, the chimney is composed of three main parts of a large pedestal, a convergent duct and a small extending duct. However, the geometries of the three parts are different that causes the description of computational domain to be complicated and increases the burden of computational processes. Besides, both effects of acceleration of flow and increment of drag resistance caused by the continuous decrement of cross section area in the convergent duct on thermal and flow mechanisms simultaneously appear that leads the analyses of thermal and flow mechanisms in the three dimensional chimney to be complex. Lots of papers [1–5] had already adopted a two dimensional modes to investigate the subject of thermal and flow mechanisms in the convergent duct and obtained available results. Regretfully, the effect of neighboring convergent walls on the thermal and flow mechanisms has difficulty to be taken into consideration in the two dimensional model. A previous study [16] had studies forced convection in a three dimensional tapered chimney and revealed the unique characteristic of the effect of neighboring convergent walls on the thermal and flow mechanism in the chimney. However, the characteristic is hardly investigated in the situation of natural convection in the three dimensional tapered chimney.

The aim of the study investigates thermal and flow phenomena of natural convection in a three dimensional tapered chimney numerically. For simulating a high temperature situation more realistically, Boussinesq assumption is no longer used and the compressibility of fluid is considered instead. Methods of Roe scheme [17], preconditioning [18], and dual time stepping [19] are adopted for solving compressible flow problems. Also in order to execute coordinate transformation and economize computational time, methods of algebraic grid generation [20] and non-reflecting boundary conditions [21] are used together. The results reveal that in addition to the increment of average Nusselt number accompanying with the decrement of cross section area due to the shape of tapered duct, the local Nusselt number in the corner region of extending duct is abruptly increased. The later phenomenon is much different from that indicated in the forced convection situation [16].

## 2. Physical model

A three dimensional tapered chimney regarded as a physical model is shown in Fig. 1. Lengths of the pedestal, tapered duct and extending duct are $l_1$, $l_2$and $l_3$, respectively. Widths of the pedestal and extending duct are $d_1$and$d_2$, respectively. The tapered angle is $\phi$ and the cross section of the chimney is square. The gravity g is downward, and the temperature and pressure of surroundings are 298 K and 101,300 Pa, respectively. The temperature of heat surfaces is constant and equal to $T_h$. The boundary condition at the inlet and outlet of chimney is non-reflecting for saving the usage of computational grids. From a point view of application, two different tapered angles of $\frac{\pi}{6}$ and $\frac{\pi}{4}$ are selected.

☆ Communicated by W.J. Minkowycz.

* Corresponding author at: Department of Mechanical Engineering, National Chiao Tung University, 1001 Ta Hsueh Road, Hsinchu, 30010, Taiwan, ROC. Tel.: +886 3 5712121x55110; fax: +886 3 5720634.
*E-mail address:* wsfu@mail.nctu.edu.tw (W.-S. Fu).

0735-1933/$ – see front matter © 2012 Elsevier Ltd. All rights reserved.
doi:10.1016/j.icheatmasstransfer.2012.01.009

**Nomenclature**

| | |
|---|---|
| $d_1$ | width of pedestal ($m$) |
| $d_2$ | width of extending duct($m$) |
| $e$ | internal energy ($J/kg$) |
| $g$ | acceleration of gravity ($m/s^2$) |
| $k$ | thermal conductivity ($W/mK$) |
| $l_1$ | length of pedestal ($m$) |
| $l_2$ | length of tapered duct ($m$) |
| $l_3$ | length of extending duct ($m$) |
| $Nu_X$ | local Nusselt number defined in Eq. (9) |
| $Nu_Y$ | loca Nusselt number defined in Eq. (1) |
| $\overline{Nu}_A$ | area average Nusselt number defined in Eq. (10) |
| P | pressure |
| Pr | Prandtl number |
| Q | mass flow ($kg/s$) defined in Eq. (11) |
| R | gas constant ($J/kg/K$) |
| Ra | Raleigh number defined in Eq. (8) |
| $t$ | time ($s$) |
| $T$ | temperature ($K$) |
| $T_0$ | temperature of surroundings ($K$) |
| $T_h$ | temperature of heat surface ($K$) |
| $u$, $v$, $w$ | velocities in $x$, $y$ and $z$ directions ($m/s$) |
| $x$, $y$, $z$ | Cartesian coordinates ($m$) |
| $X$, $Y$, $Z$ | dimensionless Cartesian coordinates |

*Greek symbols*

| | |
|---|---|
| $\gamma$ | specific heat ratio |
| $\phi$ | tapered angle of chimney |
| $\xi$, $\eta$, $\zeta$ | curvilinear coordinates |
| $\mu$ | viscosity ($N\cdot s/m^2$) |
| $\mu_0$ | Surrounding viscosity ($N\cdot s/m^2$) |
| $\rho$ | density ($kg/m^3$) |
| $\rho_0$ | surrounding density ($kg/m^3$) |
| $\tau$ | dimensionless time ($\tau = t\alpha/d_1^2$) |

For facilitating the analysis, the following assumptions are made:

1. The work fluid is ideal gas and follows the equation of state of ideal gas.
2. The magnitudes of gradients of density and pressure on the whole surfaces in the normal direction are zero.

The governing equations are derived as follows.

$$\frac{\partial U}{\partial t}+\frac{\partial F_1}{\partial x}+\frac{\partial F_2}{\partial y}+\frac{\partial F_3}{\partial z}=S \tag{1}$$

The quantities included in $U$ and $F_i$ are separately shown in the following equations.

$$U=\begin{pmatrix}\rho\\ \rho u\\ \rho v\\ \rho w\\ \rho e\end{pmatrix} \tag{2}$$

and

$$F_i=\begin{pmatrix}\rho u_i\\ \rho u_i u_1+P\delta_{i1}-\mu A_{i1}\\ \rho u_i u_2+P\delta_{i2}-\mu A_{i2}\\ \rho u_i u_3+P\delta_{i3}-\mu A_{i3}\\ (\rho e+P)u_i-\mu A_{ij}u_j-k\dfrac{\partial T}{\partial x_i}\end{pmatrix}\forall i=1(x),2(y),3(z), \tag{3}$$

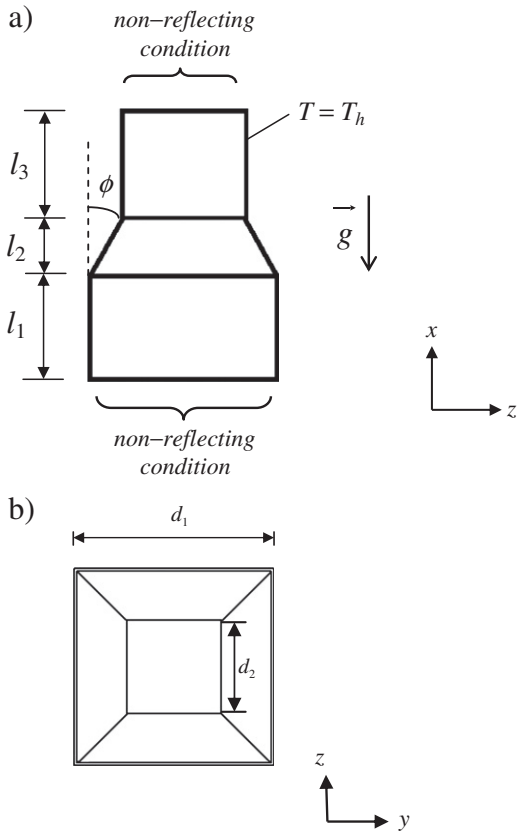


**Fig. 1.** Physical model.

where $u_1=u$, $u_2=v$, $u_3=w$ and $A_{ij}=\frac{\partial u_j}{\partial x_i}+\frac{\partial u_j}{\partial x_i}$, the ideal gas equation is written by

$$P=\rho RT \tag{4}$$

The Sutherland's law is adopted to evaluate the viscosity and the thermal conductivity.

$$\mu(T)=\mu_0\left(\frac{T}{T_0}\right)^{\frac{3}{2}}\frac{T_0+110}{T+110} \tag{5}$$

$$k(T)=\frac{\mu(T)\gamma R}{(\gamma-1)\mathrm{Pr}}$$

where $\rho_0=1.1842kg/m^3$, $g=9.81m/s^2$, $\mu_0=1.85\times10^{-5}N\cdot s/m^2$, $T_0=298K$, $\gamma=1.4$, $R=287J/kg/K$ and $\mathrm{Pr}=0.72$.

and

$$S=\begin{bmatrix}0\\ -(\rho-\rho_0)g\\ 0\\ 0\\ -(\rho-\rho_0)gu_1\end{bmatrix} \tag{6}$$

where $g=9.81m/s^2$.

To simplify the analysis, the following dimensionless variables are made.

$$X=\frac{x}{d_1},Y=\frac{y}{d_1},Z=\frac{z}{d_1}, \tag{7}$$

$$\tau = \frac{t\alpha}{{d_1}^2}$$

$$l_1 = l_3 = d_1, d_2 = \frac{3}{4}d_1$$

The variable compressibility and viscosity of the working fluid are considered, and the definition of the Rayleigh number is expressed as follows.

$$Ra = \Pr \cdot Gr = (0.72) \cdot \frac{g\beta_0 (T_h - T_0)\rho_0{}^2 d_1{}^3}{\mu_0{}^2} \quad (8)$$

## 3. Numerical method

The numerical method adopted in this work is mainly modified from that used in the previous study [16] except the factor of gravity regarded as a source term in the governing equation mentioned above. Similar derivations and computation processes are indicated in [16].

## 4. Results and Discussion

In order to increase the computational efficiency, in Fig. 2 the physical domain is transformed into the computational domain of rectangular shape by way of the method of algebraic grid generation [20].

In Fig. 3, comparison of local Nusselt numbers obtained by different grid distributions on the centerline of duct heat surface is indicated, and the grid distribution of $50 \times 50 \times 120$is selected. The definition of local Nusselt number $Nu_X$ distributed in the x direction is expressed as follows.

$$Nu_X = \frac{d_1}{k_0 (T_h - T_0)} \left[ k(T) \frac{\partial T}{\partial n} \right] \quad (9)$$

Shown in Fig. 4, the variations of average Nusselt numbers of the whole heat surface and mass flow rate at the inlet with time are indicated. The definition of average Nusselt number of the whole heat surface $\overline{Nu}_A$ and mass flow rate $Q$ at the inlet is expressed as follows.

$$Nu_Y = \frac{d_1}{k_0 (T_h - T_0)} \left[ k(T) \frac{\partial T}{\partial n} \right] \quad (10)$$

$$\overline{Nu}_A = \frac{1}{A} \int_{L_x} \int_{L_y} Nu_y dy dx \quad (11)$$

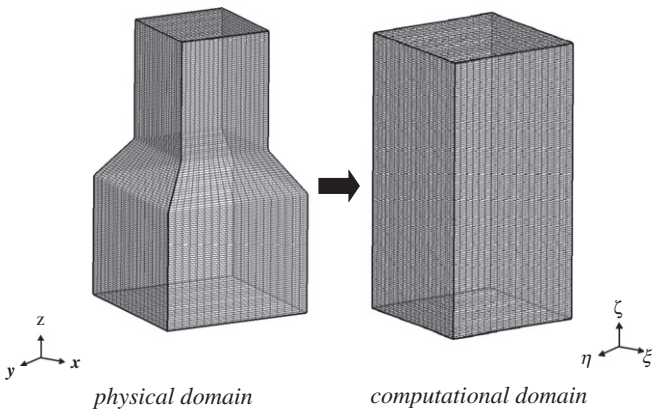


**Fig. 2.** Diagram of the coordinates transformation.

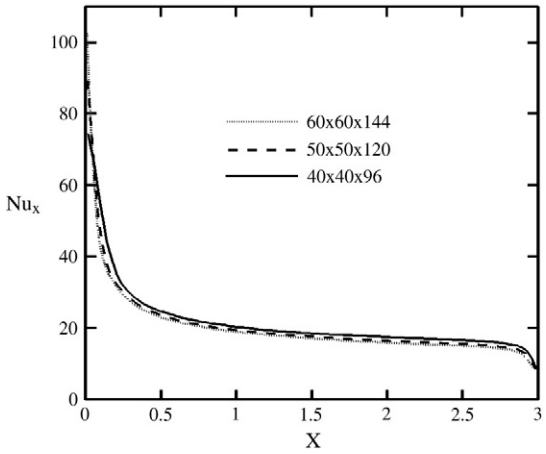


**Fig. 3.** Comparison of local Nusselt numbers on the centerline of duct heat surface. ($Ra = 2.61 \times 10^6$).

$$Q = \rho u d_1^2 \quad (12)$$

At the initial stage, the fluids in the duct are discharged to the outside of duct from both inlet and exit, because the heat wall causes decrement of the densities of fluids and increment of volume of fluids in the duct. Afterward, the buoyancy force is induced by the small densities of fluids, then part of fluids are sucked from the outside and flow into the duct via the inlet ($\overline{AB}$), and part of fluids via the outlet ($\overline{GH}$) are discharged to the outside. Besides, the cross section area of inlet and outlet are different that causes the phenomena mentioned above to happen several times repeatedly. Finally, the variable phenomena become a steady situation, and the variations of average Nusselt number and mass flow rate trend to a constant.

In Fig. 5, the distributions of velocity u on the cross sections of $\overline{AB}$, $\overline{CD}$, $\overline{EF}$ and $\overline{GH}$ are indicated, respectively. The darker the color is, the lower the velocity u displays. At the inlet $\overline{AB}$, fluids are sucked from the outside that causes velocities of fluids in the central region are faster than those near the wall region dragged by the wall. At the cross section of $\overline{CD}$, since the effect of buoyancy force on the velocity of fluid begins to appear, the velocities of fluids in the region between the central and near wall regions are faster than those in the two neighboring regions. At the cross section of $\overline{EF}$, the cross section area is contracted to the minimum area that naturally causes the velocities of fluids at this location to be accelerated. The smaller cross

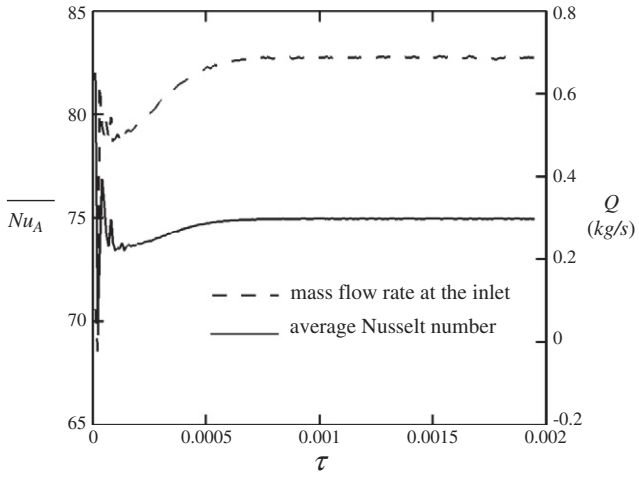


**Fig. 4.** Variations of average Nusselt numbers of the whole heat surface and mass flow rate with time. ($Ra = 2.61 \times 10^6, \phi = \frac{\pi}{6}$).

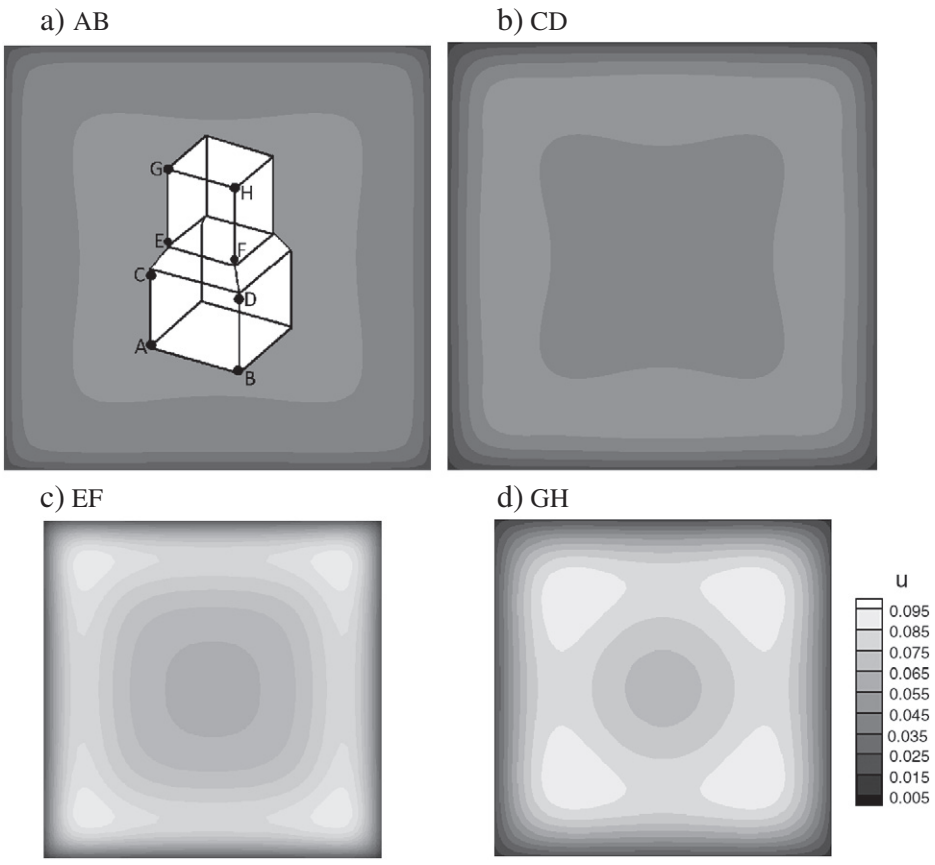


**Fig. 5.** Distributions of velocity u on *AB*, *CD*, *EF* and *GH* cross sections.( $Ra = 6.04\times10^4$, $\phi = \frac{\pi}{6}$ ).

section area leads the corner region to be more easily affected by the heat walls. As a result the velocities of fluids in the corner region are slightly faster than those in the other regions. At the outlet of $\overline{GH}$, the fluids have high velocities apparently to gather in the region close to the corner because of the buoyancy effect that causes the thickness of velocity boundary layer in the corner region to be thinner than that in the other regions. This phenomenon is advantageous to the heat transfer mechanism.

Fig. 6 indicates distributions of local Nusselt numbers $Nu_Y$'s on the $\overline{AB}$, $\overline{CD}$, $\overline{EF}$ and $\overline{GH}$ lines, respectively.

Generally, local Nusselt numbers distributed on the inlet $\overline{AB}$ line have the larger magnitude relative to those on the other location. Meanwhile the influence of buoyancy is not apparent yet, in the corner region the drag resistance caused by neighboring walls is larger than that in the central region. Then the local Nusselt number $Nu_Y$ becomes small in the corner region. The location of $\overline{CD}$ is in the downstream of the $\overline{AB}$, local Nusselt numbers distributed on the $\overline{CD}$ are naturally smaller than those on the line $\overline{AB}$. Since the line $\overline{EF}$ is located at the end of tapered duct, the cross section area on the line $\overline{EF}$ is contracted and the flow velocity is accelerated at this location. This phenomenon causes local Nusselt numbers distributed on this location to be enhanced relatively to those distributed on the line $\overline{CD}$. At the outlet $\overline{GH}$, the cross section area is constant in the extending duct and local Nusselt numbers distributed in the central region are decreased

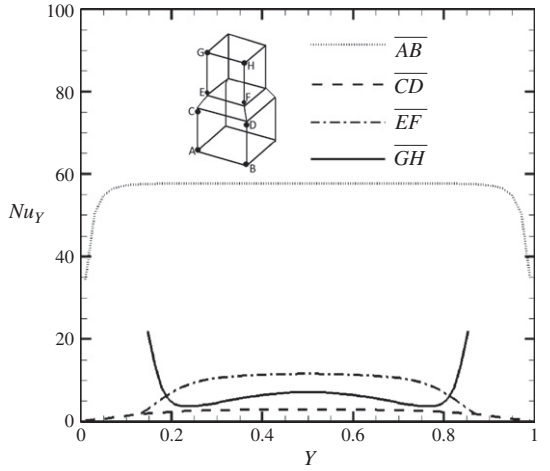


**Fig. 6.** Distributions of local Nusselt number on the $\overline{AB}$, $\overline{CD}$ , $\overline{EF}$ and $\overline{GH}$ lines. ($Ra = 6.04\times10^4$,$\phi = \frac{\pi}{6}$).

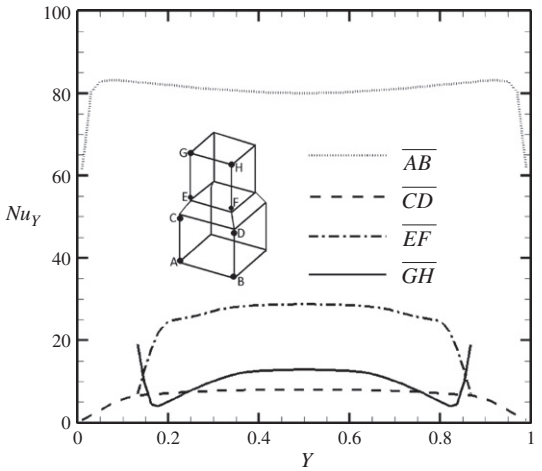


**Fig. 7.** Distributions of local Nusselt number on the $\overline{AB}$, $\overline{CD}$ , $\overline{EF}$ and $\overline{GH}$ lines. ($Ra = 2.61\times10^6$,$\phi = \frac{\pi}{6}$).

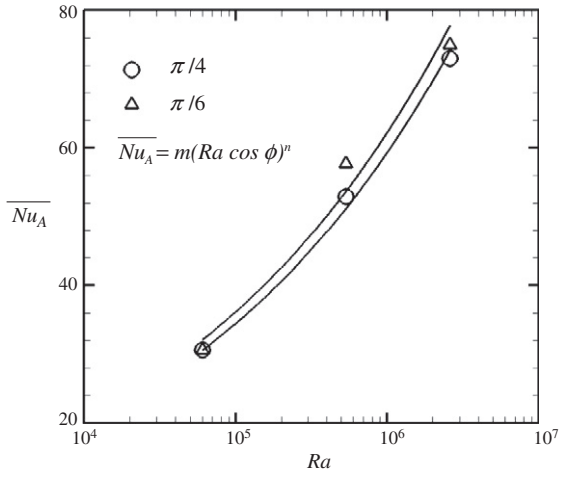


**Fig. 8.** Comparison of the area average Nusselt numbers with a correlation equation for $\phi = \frac{\pi}{6}$ and $\phi = \frac{\pi}{4}$ situations.

and smaller than those distributed on the line $\overline{EF}$. However, close to the corner region the influence of the increment of the buoyancy force induced by the neighboring heat walls is more effective than that of the increment of drag resistance induced by the neighboring heat walls. As a result, local Nusselt numbers close to the corner region are larger than those of the central region. This phenomenon is much different from that shown in the previous study [16].

In Fig. 7, Rayleigh number increases to $2.61\times10^6$. Basically, those phenomena of distributions of local Nusselt numbers are similar to those indicated in Fig. 6. The whole magnitudes shown in this figure are larger than those shown in Fig. 6.

Fig. 8 indicates comparisons of area average Nusselt numbers with a correlation equation. The correlation equation is expressed as follows.

$$\overline{Nu_A} = m(Ra\cos\phi)^n \tag{13}$$

where m = 2.495 and n = 0.235 for $6.04\times10^4 \le Ra \le 2.61\times10^6$ and $\frac{\pi}{6} \le \phi \le \frac{\pi}{4}$.

The maximum deviation of both results is not larger than 7%.

## 5. Conclusions

An investigation of compressible natural convection in a three dimensional tapered chimney is performed numerically. The conclusions are drawn as follows.

1. In the extending duct, local Nusselt numbers in the corner region are larger than those in the central region. This is a characteristic of the natural convection that is rather different from that of the forced convection.
2. Both results obtained by numerical computation and correlation equation have good agreements.

## Acknowledgement

The authors gratefully acknowledge the support of the Natural Science Council, Taiwan, ROC under Contact NSC97-2221-E-009-144.

## References

[1] E.M. Sparrow, R. Ruiz, Experiments on Natural Convection in Divergent Vertical Channels and Correlation of Divergent, Convergent, and Parallel-Channel Nusselt Numbers, International Journal Heat and Mass Transfer 31 (1988) 2197–2205.
[2] E.M. Sparrow, R. Ruiz, L.F.A. Azevedo, Experimental and Numerical Investigation of Natural Convection in Convergent Vertical Channel, International Journal Heat and Mass Transfer 31 (1988) 907–915.
[3] C.C. Su, H. Lin, Heat Transfer and Pressure Drop Characteristics of Flow in Convergent and Divergent Ducts, International Journal of Energy Research 15 (1991) 7581–7591.
[4] C.C. Su, R.H. Lin, Experimental Studies on Flow in Convergent and Divergent Ducts of Rectangular Cross Section, International Journal of Energy Research 21 (1997) 77–86.
[5] K.D. Kihm, J.H. Kim, L.S. Fletcher, Investigation of Natural Convection in Heat Transfer in Converging Channel Flow Using a Specklegram Technique, Journal of Heat Transfer 115 (1993) 140–148.
[6] K.R. Mutama, H. Iacovides, The Investigation of Developing Flow and Heat Transfer in a Long Converging Duct, Journal of Heat Transfer 115 (1993) 897–903.
[7] S.A.M. Said, Investigation of Natural Convection in Convergent Vertical Channels,, International Journal of Energy Research 20 (1996) 559–567.
[8] J.S. Shalash, J.D. Tarasuk, D. Naylor, Experimental and Numerical Studies of Natural Convection Heat Transfer in Vertical Converging Channel Flows, Proceeding of Fourth Experimental Heat Transfer, Fluid Mechanics and Thermodynamics (1997) 2167–2174.
[9] N. Bianco, S. Nardini, Numerical Analysis of Natural Convection in Air in a Vertical Convergent Channel with Uniformly Heated Conductive Walls, International Communications in Heat and Mass Transfer 32 (2005) 758–769.
[10] N. Bianco, L. Langellotto, O. Manca, S. Nardini, Thermal Design and Optimization of Vertical Convergent Channels in Natural Convection, Applied Thermal Engineering 26 (2006) 170–177.
[11] N. Bianco, O. Manca, S. Nardini, Experimental Investigation on Natural Convection in a Convergent Channel With Uniformly Heated Plates, International Journal of Heat and Mass Transfer 50 (2007) 2772–2786.
[12] A.S. Kaiser, B. Zamora, A. Viedma, Correlation for Nusselt Number in Natural Convection in Vertical Convergent Channels at Uniform Wall Temperature by a Numerical Investigation, International Journal of Heat and Fluid Flow 25 (2004) 671–682.
[13] A. Andreozzi, B. Buonomo, O. Manca, Numerical Study of Natural Convection in Vertical Channels with Adiabatic Extensions Downstream, Numerical Heat Transfer A 47 (2005) 741–762.
[14] A. Andreozzi, B. Buonomo, O. Manca, Thermal Management of a Symmetrically Heated Channel–Chimney System, International Journal of Thermal Sciences 48 (2009) 475–487.
[15] A. Andreozzi, B. Buonomo, O. Manca, Thermal and Fluid Dynamic Behaviors in Symmetrical Heated Channel-Chimney Systems, International Journal of Numerical Methods Heat Fluid Flow 20 (2010) 811–833.
[16] W.S. Fu, W.H. Wang, Y. Huang, C.G. Li, An Investigation of Compressible Forced Convection in a Three Dimensional Tapered Chimney by CUDA Computation Platform, International Journal of Heat Mass Transfer 54 (2011) 3420–3430.
[17] P.L. Roe, Approximation Riemann Solver, Parameter Vectors, and Difference Schemes, Journal of Computational Physics 43 (1981) 357–372.
[18] J.M. Weiss, W.A. Simth, Preconditioning Applied to Variable and Constants Density Flows, AIAA 33 (1995) 2050–2056.
[19] X.F. Xu, J.S. Lee, R.H. Pletcher, A compressible finite volume formulation for large eddy simulation of turbulent pipe flows at low Mach number in Cartesian coordinates, Journal of Computational Physics 203 (2005) 22–48.
[20] K.A. Hoffmann, S.T. Chiang, Computational Fluid Dynamics for Engineering, Engineering Education System, Wichita, Kan, 1993.
[21] T.J. Poinsot, S.K. Lele, Boundary Conditions for Navier–Stokes, Journal of Computational Physics 101 (1992) 104–129.